

Bloch-Lorentz magnetoresistance oscillations in delafossites

K. Vilkelis^{1*, 2}, L. Wang², A. Akhmerov²

¹ Qutech, Delft University of Technology, Delft 2600 GA, The Netherlands

² Kavli Institute of Nanoscience, Delft University of Technology, Delft 2600 GA, The Netherlands

* kostasvilkelis@gmail.com

June 21, 2021

Abstract

Recent measurements of the out-of-plane magnetoresistance of delafossites (PdCoO_2 and PtCoO_2) observed oscillations which closely resemble the Aharonov-Bohm effect. We develop a semiclassical theory of these oscillations and show that they are a consequence of the quasi-2D dispersion of delafossites. We observe that the Lorentz force created by an in-plane magnetic field makes the out-of-plane motion of electrons oscillatory, similarly to Bloch oscillations. The visibility of these Bloch-Lorentz oscillations is limited by sample wall scattering. Therefore, the aspect ratio of the sample controls the intensity of scattering. Our theory offers a way to design an experimental geometry that is better suited for probing the phenomenon and to investigate the out-of-plane dynamics of ballistic quasi-two-dimensional materials.

Contents

1	Introduction	2
2	Ballistic in-plane model in the weak out-of-plane coupling limit	3
3	Results	5
3.1	In-plane magnetic field	5
3.2	Realistic sample geometry	7
3.3	Out-of-plane magnetic field	9
4	Summary	11
	References	11

1 Introduction

Known since the discovery of mineral CuFeO_2 by Friedel in 1873, delafossites are materials with the general formula ABO_2 [1,2]. Delafossites are naturally occurring layered structures of alternating conductive A layer and insulating BO_2 layer with the overall $R\bar{3}m$ space group [3]. These materials are considered to be 2D owing to their weak interlayer coupling which results in a near cylindrical Fermi surface [4, 5]. Of particular interest are PdCoO_2 and PtCoO_2 which were first synthesized and characterized at room temperature in 1971 by Shannon *et al.* [2, 3, 6]. Even though nearly 50 years have passed since then, the area of research is still very active due to the delafossite's impressive electronic transport properties [7]. At room temperature, it was shown that the conductivity of PdCoO_2 is $2.6 \mu\Omega \text{ cm}$, very close to that of elemental Copper [8]. Part of the reason for such large conductivity is the high Fermi velocity $7.5 \times 10^5 \text{ m s}^{-1}$ [8]. Another reason is their exceptional mean-free path at 4K which exceed $20 \mu\text{m}$ [8]. Such value of mean-free path is accredited mostly to anomalously clean nature of delafossites and orbital-momentum locking [9, 10]. Overall, all of these properties of delafossites make them a good platform to study mesoscopic ballistic transport [11].

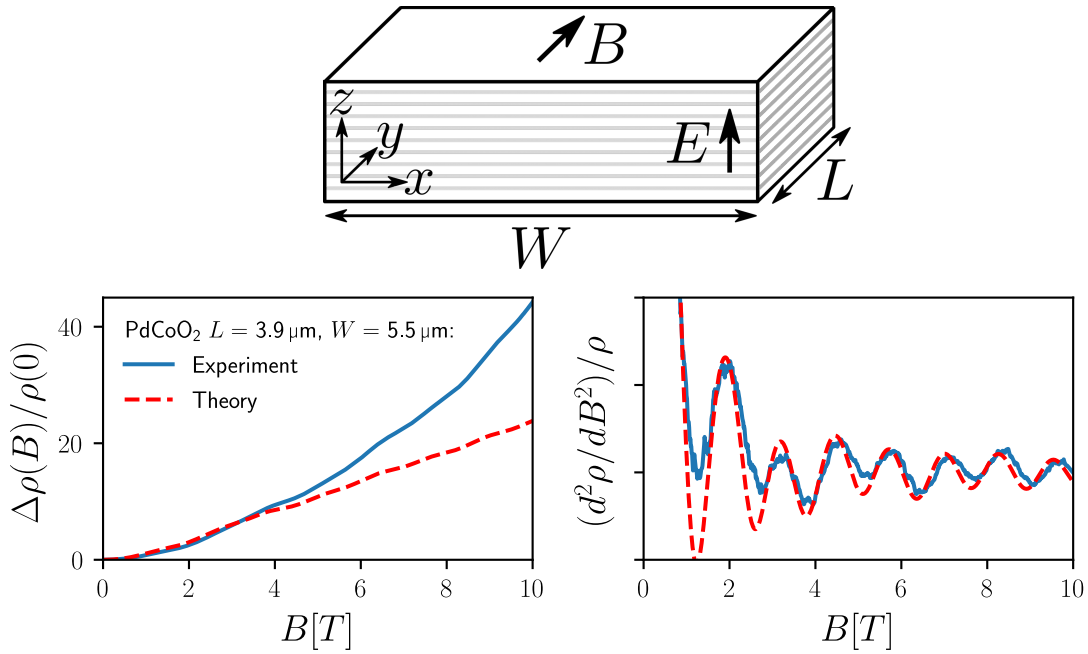


Figure 1: PdCoO_2 magnetoresistance experimental set up (top) and results (solid blue lines) obtained by Putzke *et al.* [12]. The semiclassical fit (dashed red lines) was obtained by modelling the finite size PdCoO_2 sample.

Recent experiments looked into the out-of-plane transport of PdCoO_2 [12], the setup and magnetoconductance results shown by Fig. 1. Magnetoconductance was measured with the magnetic field applied in the plane of the delafossite layers and the current passing out-of-plane. Surprisingly, the results showed oscillations with a magnetic field whose nature is not clear. At first sight, the oscillations follow similar behaviour to the Aharonov-Bohm effect. The frequency is controlled by the flux quanta going through the loop defined between

the adjacent conducting atomic layers and the width of the sample. Despite the apparent similarity with the Aharonov-Bohm, it is not able to explain these observations. Firstly, it would require hopping between layers only at the edges of the sample. Furthermore, these loops would need to be somehow decoupled. Lastly, the temperature dependence shows these oscillations persist up until 60 K, which would imply an impressive resilience of the coherence to temperature. A better explanation is required. A calculation of the oscillations by Putzke *et al.* relies on a tight-binding Hofstadter model with Kubo formula. The approach reproduces the results, however, due to its numerical nature, offers limited insight into the nature of the phenomenon [12].

In the following paper, we use the semiclassical theory to explain the magnetoconductance results. We explain the oscillations as a consequence of the shape of the semiclassical trajectories rather than an interference pattern. Therefore, the quasi-2D energy dispersion of delafossites is the main ingredient needed in reproducing the oscillations observed in experiments.

Measurements on delafossites' mean free path suggest a fully ballistic model [8]. However, we find that such a model describes oscillations with full visibility, in contradiction to the results by Putzke *et al.* [12]. We propose scattering at the sample walls as a possible mechanism to resolve this contradiction.

We find that boundaries alter the electronic trajectories and therefore complicate the analysis. We predict that by increasing sample's length along the direction of the magnetic field, the results of the theory converge with experimental findings.

2 Ballistic in-plane model in the weak out-of-plane coupling limit

Delafossites have large carrier density and are highly conductive [13, 14]. Therefore it is a metallic system in which interference effects should not play a deciding role.

Delafossites' conduction band is well approximated by the energy dispersion

$$\varepsilon(\mathbf{k}) = \varepsilon_{\parallel}(\mathbf{k}_{\parallel}) - t_z \cos(k_z c'), \quad (1)$$

where $\varepsilon_{\parallel}(\mathbf{k}_{\parallel})$ is hexagonal in-plane dispersion [8, 14, 15], c' is the interlayer distance and t_z is the interlayer hopping. The interlayer dispersion is weak [4, 8] i.e. t_z is much smaller than the in-plane bandwidth. This motivates a perturbative approach in terms of t_z used throughout the paper.

We compute electron density $f(\mathbf{r}, \mathbf{k}, t)d^3\mathbf{k}$ at position \mathbf{r} , time t and momentum \mathbf{k} by using the Boltzmann equation. We separate electron density into the equilibrium part (Fermi-Dirac distribution) f^0 and non-equilibrium part δf . Further simplification is achieved by setting

$$\delta f(\mathbf{r}, \mathbf{k}) = -g(\mathbf{r}, \mathbf{k}) \frac{\partial f^0}{\partial \varepsilon}, \quad (2)$$

where at zero temperature $\frac{\partial f^0}{\partial \varepsilon}$ becomes a Dirac delta function centered around Fermi energy. The resulting steady state linearised Boltzmann equation reads [16]

$$\mathbf{v} \cdot \nabla_{\mathbf{r}} g - \frac{e}{\hbar} (\mathbf{v} \times \mathbf{B}) \cdot \nabla_{\mathbf{k}} g - e v_z \mathcal{E}_z = \mathcal{L}g, \quad (3)$$

where \mathbf{v} is the velocity, e is the elementary charge, \hbar is the reduced Planck constant, \mathbf{B} is the magnetic field, \mathcal{E}_z is the electric field along the out-of-plane direction and $\mathcal{L}g$ is the linearised collision integral. The boundary conditions at the boundaries $x = 0$ ($\xi = 1$) and $x = W$ ($\xi = -1$) are

$$|v_x(\mathbf{k}_{\parallel})|g(\mathbf{r}_B, \mathbf{k}) = \int_{v_x(\mathbf{k}'_{\parallel})\xi < 0} K(\mathbf{k}', \mathbf{k}) \times |v_x(\mathbf{k}'_{\parallel})| g(\mathbf{r}_B, \mathbf{k}') d^3k', \quad (4)$$

where \mathbf{r}_B is the location of the boundary and K is the boundary scattering kernel. Because Eqs (3) and (4) are translationally invariant along y and z , the solution $g(x, \mathbf{k})$ is invariant as well.

We expand g in Eq. (3) as a series to first order in t_z :

$$g(\mathbf{r}, \mathbf{k}) \approx g_0(\mathbf{r}, \mathbf{k}) + g_1(\mathbf{r}, \mathbf{k}), \quad (5)$$

where g_0 does not depend on t_z and $g_1 \propto t_z$. With the magnetic field inside the yz plane $\mathbf{B} = (0, B_y, B_z)$, the zeroth order equation is

$$v_x \frac{\partial g_0}{\partial x} - \frac{e}{\hbar} (\mathbf{v}_{\parallel} \times \mathbf{B}) \cdot \nabla_{\mathbf{k}} g_0 = \mathcal{L}g_0, \quad (6)$$

where \mathbf{v}_{\parallel} is in-plane velocity. Equation (6) describes an electron in a magnetic field with no external forces capable of generating a steady non-equilibrium distribution. Furthermore, the scattering term ensures that the steady state solution is $g_0 = 0$. Therefore, to first order in t_z linearised Boltzmann equation is

$$v_x \frac{\partial g}{\partial x} - \frac{e}{\hbar} (\mathbf{v}_{\parallel} \times \mathbf{B}) \cdot \nabla_{\mathbf{k}} g - ev_z \mathcal{E}_z = \mathcal{L}g. \quad (7)$$

Since $g \propto t_z$, it is sufficient to approximate \mathcal{L} to zeroth order in t_z .

Integrating Eq. (7) over k_z within the 1st Brillouin zone, we obtain an equation identical to Eq. (6), but with g_0 replaced by $g_{\parallel}(\mathbf{r}, \mathbf{k}_{\parallel}) \equiv \int_{\text{BZ}} g(\mathbf{r}, \mathbf{k}) dk'_z$. Therefore, the in-plane current of electrons vanishes in the steady state:

$$\int_{\text{BZ}} g(\mathbf{r}, \mathbf{k}) dk_z = 0. \quad (8)$$

Because the samples in the work by Putzke *et al.* [12] are formed using focused ion beam milling and thus have amorphous edges, and because the weak out-of plane dispersion, we focus on the boundary conditions that randomize the out-of-plane momentum k_z . In this limit the boundary scattering kernel K does not depend on k_z , and substitution of Eq. (8) in Eq. (4) yields the following:

$$g(x_B, y, z, \mathbf{k}) = 0, \quad (9)$$

$$x_B = \begin{cases} 0 & k_x > 0 \\ W & k_x < 0. \end{cases}$$

While this approximation simplifies the simulations, and is likely realistic, we note that the appearance of oscillations in this limit is not sensitive to the boundary conditions.

To analyse experimental observations, we compute the current along z

$$I_{zz} = e \int_0^W dx \int_0^L dy \iiint_{\text{BZ}} f(\mathbf{r}, \mathbf{k}) v_z(\mathbf{k}) d\mathbf{k}. \quad (10)$$

We express the out-of-plane conductivity $\sigma_{zz} = I_{zz}/(\mathcal{E}_z WL)$ at zero temperature by substituting Eq. (2) into Eq. (10):

$$\sigma_{zz} = \frac{e}{W\mathcal{E}_z} \int_0^W dx \iiint_{\text{BZ}} \delta(\varepsilon - \varepsilon_F) g(x, \mathbf{k}) v_z(\mathbf{k}) d\mathbf{k}, \quad (11)$$

where ε_F is the Fermi energy. We compute the lowest nonvanishing contribution in t_z to conductivity. Since $g_0 = 0$, we approximate the energy $\varepsilon(k_x, k_y, k_z) \approx \varepsilon_{\parallel}$ only to zeroth order in t_z . We switch to cylindrical coordinates in k-space (x, k, θ, k_z) where k is the in-plane wavevector length and θ is the azimuth. The conductivity to the lowest order in t_z is

$$\sigma_{zz} = \frac{e}{W\mathcal{E}_z\hbar} \int_0^{2\pi} \int_0^W \int_{-\frac{\pi}{c'}}^{\frac{\pi}{c'}} \frac{k_F(\theta)}{v_R(\theta)} g(x, k_F(\theta), \theta, k_z) \times v_z(k_z) d\theta dx dk_z, \quad (12)$$

where

$$v_R(\theta) = \frac{1}{\hbar} \frac{\partial \varepsilon_{\parallel}}{\partial k}, \quad (13)$$

and $k_F(\theta)$ is the Fermi wavevector $\varepsilon(k_F(\theta), \theta) = \varepsilon_F$.

3 Results

3.1 In-plane magnetic field

Because the mean free path of delafossites is larger than the sample size [12], to illustrate the origin of the oscillations we first neglect scattering $\mathcal{L}g = 0$. With in-plane magnetic field $\mathbf{B} = (0, B_y, 0)$, the Boltzmann Eq. (7) reduces to

$$v_x \frac{\partial g(x, v_x, k_z)}{\partial x} - v_x \frac{eB_y}{\hbar} \frac{\partial g(x, v_x, k_z)}{\partial k_z} - e\mathcal{E}_z v_z = 0, \quad (14)$$

where $g(x, v_x, k_z)$ only depends on k_x and k_y through $v_x(k_x, k_y)$ as seen in Eq. (14).

Solution to Eq. (14) fulfilling the boundary conditions of Eq. (9) is

$$g(x, v_x, k_z) = \frac{-t_z \mathcal{E}_z}{B_y v_x} \left[\cos(k_z c') - \cos\left(k_z c' + \frac{\omega B_y}{W} x_B\right) \right], \quad (15)$$

with:

$$\omega = \frac{e}{\hbar} c' W, \quad x_B = \begin{cases} x & \text{for } v_x > 0 \\ x - W & \text{for } v_x < 0. \end{cases} \quad (16)$$

We substitute Eq. (15) into Eq. (12), and obtain the conductivity along z

$$\sigma_{zz} = \frac{e\pi t_z^2}{\omega \hbar B_y^2} (1 - \cos(\omega B_y)) \int_0^{2\pi} \frac{k_F(\theta)}{v_x(\theta) v_R(\theta)} d\theta. \quad (17)$$

When the magnetic field is of the form $\mathbf{B} = (0, B_y, B_z)$, the k_z dependence on x is

$$k_z(x) = k_{z0} + \frac{e}{\hbar} B_y x. \quad (18)$$

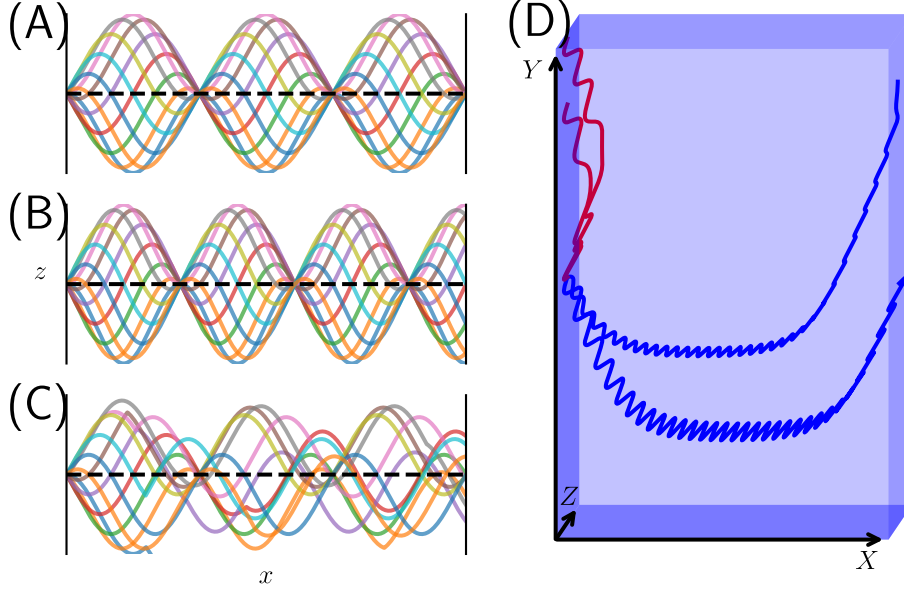


Figure 2: (A) Trajectories with oscillations commensurate to the sample width due to an in-plane magnetic field. Different curves indicate the different initial phase of the trajectory. (B) Same as in (A), but the in-plane magnetic field is chosen to give incommensurate oscillations. (C) Same as in (A), but with scattering present. (D) Trajectories due to an out-of-plane magnetic field. Blue lines are boundary-to-boundary trajectories whereas the red lines are edge-localized trajectories. Only the boundary-to-boundary trajectories produce current oscillations due to a net k_z drift throughout the trajectory.

This results in the electron trajectory

$$z(x) = \frac{t_z}{\hbar v_x} \left[\cos \left(k_{z0} + \frac{e}{\hbar} B_y x \right) - \cos(k_{z0}) \right]. \quad (19)$$

All trajectories have a similar oscillatory vertical displacement as a function of x , shown in Fig. 2(A,B). *The universal trajectory shape is a result of the k_z advancing over the complete out-of-plane Brillouin zone, similar to Bloch oscillations [17], however because of the magnetic origin of the momentum drift, k_z has a universal dependence on x regardless of the in-plane trajectory.* When the oscillation period is commensurate with the sample width, all trajectories have a zero net vertical displacement over the time of flight, and therefore carry no current as shown in Fig. 2(A). At the same time, the vertical displacement of different trajectories—and therefore the current—is maximal when a half-integer number of oscillation periods fits into the sample width as shown in Fig. 2(B). Because the contribution of every trajectory to the conductance has the same magnetic field dependence, as seen in Eq. (17), this minimal model yields an oscillatory conductance with a correct frequency, but full visibility of the oscillations in contrast to the experimental data.

In the regime of linearised Boltzmann equations with translational invariance along y and z , the only possible generalisation is addition of scattering which randomizes the vertical displacement and suppresses the visibility of the oscillations due to the trajectory shape as

shown in Fig. 2 (C). We assume a simple relaxation time approximation model:

$$\mathcal{L}g = -\frac{g(k, \theta, k_z)}{\tau}, \quad (20)$$

where τ is the relaxation time.

We now substitute Eq. (20) into the right hand side of Eq. (14) and obtain linearised Boltzmann equation with relaxation whose solution is

$$g(x, \theta, k_z) = \frac{\mathcal{E}_z \tau e c' t_z}{\hbar (B_y^2 \phi^2 + 1)} \left(B_y \phi \cos(k_z c') + \sin(k_z c') \right. \\ \left. - \exp\left(-\frac{x_B}{l}\right) \left[B_y \phi \cos\left(k_z c' + \frac{\omega B_y}{W} x_B\right) + \sin\left(k_z c' + \frac{\omega B_y}{W} x_\theta\right) \right] \right), \quad (21)$$

with:

$$l(\theta) = \tau v_x(\theta), \quad \phi(\theta) = \frac{e}{\hbar} c' l(\theta). \quad (22)$$

We substitute Eq. (21) into Eq. (12), and obtain conductivity per unit azimuth

$$\sigma_{zz}(B_y) = \frac{\tau e^2 t_z^2 c' \pi}{\hbar^2} \int_0^{2\pi} \frac{k_F(\theta)}{v_R(\theta) (B_y^2 \phi^2 + 1)^2} \times \left(1 - r + (B_y \phi)^2 r + (B_y \phi)^2 + r \exp\left(-\frac{1}{r(\theta)}\right) \right. \\ \left. \times \left[(1 - B_y^2 \phi^2) \cos(\omega B_y) - 2 B_y \phi \sin(\omega B_y) \right] \right) d\theta, \quad (23)$$

with

$$r = l(\theta)/W. \quad (24)$$

We recover a simple Drude model B^2 resistivity scaling [18] in Eq. (23) by removing the boundaries, $W \rightarrow +\infty$, which removes the second term in Eq. (23). We conclude that the addition of boundaries alters the overall conductance profile.

3.2 Realistic sample geometry

The simple model in Eq.(23) requires a mean free path of $l(0) \approx 4.4 \mu\text{m}$ in order to explain the experimental oscillations observed in delafossites, much shorter than the expected bulk value of $20 \mu\text{m}$ [8]. Therefore, the dominant source of scattering must originate from the boundaries. In the experimental setup by Putzke *et al.* [12], the sample has a low aspect ratio with sample length shorter than the width $W > L$. As a result, we expect the boundaries along the length of the sample to alter the semiclassical trajectories.

To solve the Boltzmann equation for a realistic sample geometry we use that scattering Eq. (20) does not mix non-equilibrium electron densities along different ballistic trajectories. We therefore compute g along each ballistic electron trajectory separately. The trajectories follow the semiclassical equations of motion:

$$\hbar \frac{d\mathbf{r}(t)}{dt} = \nabla_{\mathbf{k}} \varepsilon(\mathbf{k}), \\ \hbar \frac{d\mathbf{k}(t)}{dt} = -e\mathbf{v}(t) \times \mathbf{B}. \quad (25)$$

We parameterize each trajectory originating at a sample boundary through its initial coordinate and wave vector $\mathbf{r}_0 = (x_0, y_0, z_0)$ and $\mathbf{k}_0 = (k_0 \cos \theta_0, k_0 \sin \theta_0, k_{z,0})$. In the rectangular geometry we consider all the four boundaries: $x = 0$, $x = W$, $y = 0$, $y = L$, and choose the initial angle θ_0 so that \mathbf{k}_0 points inwards of the sample. At a sufficiently high out-of-plane magnetic field, bulk cyclotron orbits appear that do not intersect with sample boundaries. We disregard these trajectories because they do not contribute to the h/e magnetoresistance oscillations, however extending our approach to those trajectories is straightforward.

Using Eq. (25), we obtain the evolution of g along a single trajectory

$$\frac{\partial g(t, \mathbf{r}_0, \mathbf{k}_0)}{\partial t} = \mathbf{v} \cdot \nabla_{\mathbf{r}} g - \frac{e}{\hbar} (\mathbf{v} \times \mathbf{B}) \cdot \nabla_{\mathbf{k}} g. \quad (26)$$

Substituting Eq. (26) and Eq. (20) into Eq. (7), we obtain the Boltzmann equation along a single trajectory

$$\frac{\partial g(t, \mathbf{r}_0, \mathbf{k}_0)}{\partial t} - e\mathcal{E}_z v_z(k_z(t)) = -\frac{g(t, \mathbf{r}_0, \mathbf{k}_0)}{\tau}, \quad (27)$$

with solution

$$g(t, \mathbf{r}_0, \mathbf{k}_0) = -e\mathcal{E}_z \int_0^t v_z(k_z(t')) \times \exp\left(-\frac{(t-t')}{\tau}\right) dt'. \quad (28)$$

By changing the variables in Eq. (12) to the trajectory coordinate system (t, θ_0, k_{z0}) , σ_{zz} has the form

$$\sigma_{zz} = \frac{-e}{W\mathcal{E}_z\hbar} \oint dr_0 \int_{\theta_{min}}^{\theta_{max}} d\theta_0 \int_0^{t_B(\theta_0, \mathbf{r}_0)} dt' \frac{k_F(\theta(\theta_0, t))}{v_R(\theta(\theta_0, t))} J(t', \theta_0) \times \int_{-\pi/c}^{\pi/c} dk_{z0} g(\mathbf{r}_0, t', \theta_0, k_{z0}) v_z(\mathbf{r}_0, t', \theta_0, k_{z0}), \quad (29)$$

with the Jacobian determinant J is

$$J(t', \theta_0) = \left(\frac{\partial \theta}{\partial t'} \bigg|_{t'=0} \right)^{-1} \frac{\partial \theta}{\partial t'} v_x(0, \theta_0). \quad (30)$$

In Eq. (29), the r_0 integral is over the sample boundary and $t_B(\theta)$ is the time that the trajectory hits a boundary. The integral over θ_0 includes the contributions of all trajectories within the sample.

We solve Eq. (29) numerically with an in-plane magnetic field B_y and without bulk scattering $\tau \rightarrow \infty$. See Ref. [19] for the numerical code and the resulting data. The magnetoresistance of a sample with fixed width W and variable length L is shown in Fig. 3. Because the side boundaries enhance scattering, we observe that the magnetoresistance oscillation visibility drop with the aspect ratio L/W . Using the geometry of the sample of Ref. [12], we confirm that the computed relative magnitude of the oscillations is in a quantitative agreement with the measured values, however the overall resistance profile is somewhat different as shown in Fig. 1. The possible reasons for this disagreement are residual bulk scattering, minor misalignment of the magnetic field or inhomogeneity of the sample along the z -direction.

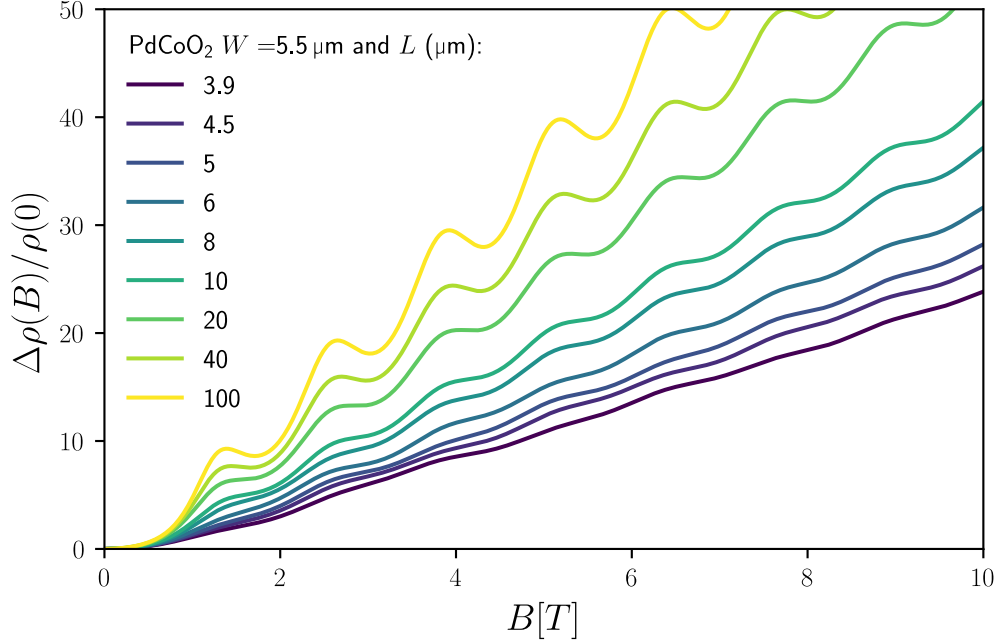


Figure 3: Semiclassical predictions of PdCoO₂ magnetoresistance with variable sample aspect ratio.

3.3 Out-of-plane magnetic field

In the presence of an out-of-plane magnetic field B_z , the in-plane projection of each trajectory is a rotated and rescaled hexagonal Fermi surface, while the out of plane motion follows the same oscillatory pattern, with the resulting motion shown in Fig. 2 (D). We use the integral form of the Boltzmann Eq. (29) to find the magnetoresistance response. In this case, we neglect the top and bottom boundaries and instead model their effect with a finite relaxation time τ . We choose the starting point of each trajectory as $t = 0$, so that its initial conditions are $\mathbf{r}_0 = (x_0, y_0, z_0)$ and $\mathbf{k}_0 = (k_0 \cos \theta_0, k_0 \sin \theta_0, k_{z,0})$. Here $x_0 = 0$ and $-\pi/2 < \theta_0 < \pi/2$ at the left boundary, while $x_0 = W$ and $\pi/2 > \theta_0 > 3\pi/2$ at the right boundary.

There are two types of trajectories along which Eq. (29) is integrated: boundary-to-boundary and edge-localized trajectories as shown in Fig. 2(D). These two trajectories have different contributions to the conductance profile. Conductance oscillations are controlled only by the boundary-to-boundary trajectory because it results in net k_z drift according to Eq. (18). On the other hand, the edge-localized trajectory does not affect the conductance oscillations as a result of the absence of k_z drift. Once the cyclotron orbits become smaller than W , which happens at

$$B_z > \left(\frac{2\hbar k_F}{eW} \right), \quad (31)$$

with k_F the Fermi wavevector, the boundary-to-boundary trajectories disappear, and so does the oscillatory contribution to conductance.

We perform numerical integration of Eq.(29), with the result shown in Fig. 4. The model qualitatively agrees with the experimental data at the small tilt angles from the xy -plane. However, the disagreement increases with B_z , likely due to our calculation assuming transla-

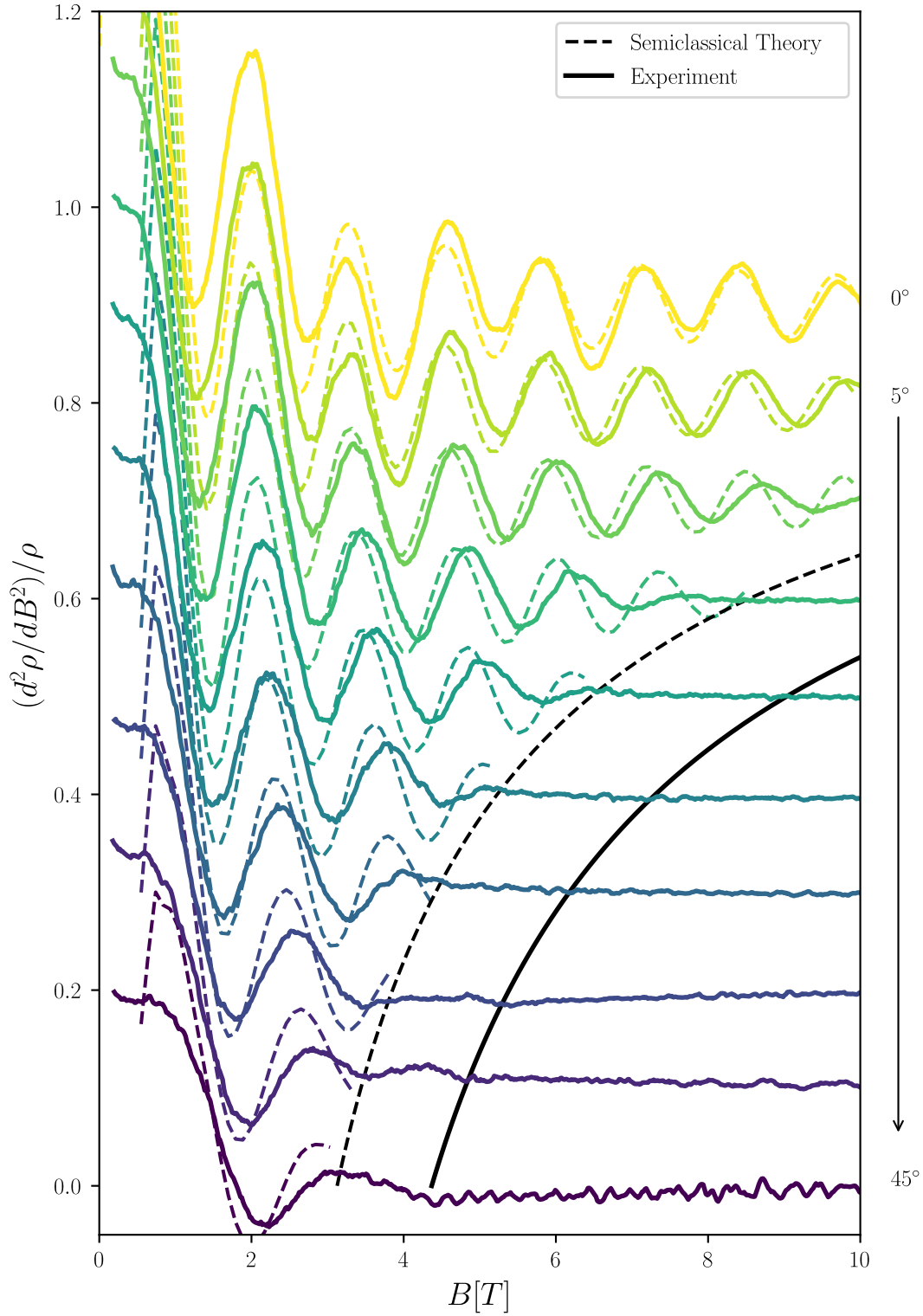


Figure 4: Numerical results from the semiclassical theory (dashed lines) with $l(0) = 4.4\mu\text{m}$ compared to the experimental (solid lines) magnetoresistance results by Putzke *et al.* [12] for magnetic field tilted out-of-plane by 5° steps. Black lines indicate the critical field when the cyclotron orbit fits inside the sample. The critical field value is determined by the shorter side of the sample. In the experiment, this is the length of the sample L , whereas in the semiclassical fit it is the width of the sample W .

tional invariance along y direction. This is likely a crude approximation because the sample length L is shorter than W in the experiment. The extension of the theory to a realistic sample geometry is straightforward—especially since one may still compute g for every trajectory independently—but it strongly increases the computational costs, and therefore we consider it unjustified for the purposes of our study.

4 Summary

In summary, we demonstrated that the observed magnetoresistance of delafossite materials is explained by the Bloch-like oscillations of the out-of-plane electron trajectories. These Bloch-Lorentz oscillations arise from the quasi-2D dispersion of these materials combined with the nearly ballistic motion of the electrons. Our identification enables a way of probing the out-of-plane momentum relaxation in quasi-2D materials as well as out-of-plane dispersion relation.

Acknowledgements

We would like to thank Ady Stern, Veronika Sunko, and Maja Bachmann for the helpful discussions in the early stages of the project. Also, we are grateful to Philip J.W. Moll and Carsten Putzke for sharing with us their experimental findings and subsequent consultations.

A.A. formulated the project idea. K.V. developed the theory, carried out the numerical simulations, and analyzed the data with input from the other authors. The manuscript was written jointly by K.V. and A.A. with input from L.W.

This work was supported by the NWO VIDI Grant (016.Vidi.189.180), an ERC Starting Grant 638760 and European Union's Horizon 2020 research and innovation programme FE-TOpen Grant No. 828948 (AndQC).

References

- [1] C. Friedel, *Sur une combinaison naturelle des oxydes de fer et de cuivre, et sur la reproduction de l'atacamite*, Sciences Academy **77**, 211 (1873).
- [2] R. D. Shannon, D. B. Rogers and C. T. Prewitt, *Chemistry of noble metal oxides. i. syntheses and properties of abo₂ delafossite compounds*, Inorganic Chemistry **10**(4), 713 (1971).
- [3] R. D. Shannon, C. T. Prewitt and D. B. Rogers, *Chemistry of noble metal oxides. ii. crystal structures of platinum cobalt dioxide, palladium cobalt dioxide, copper iron dioxide, and silver iron dioxide*, Inorganic Chemistry **10**(4), 719 (1971).
- [4] K. P. Ong, J. Zhang, J. S. Tse and P. Wu, *Origin of anisotropy and metallic behavior in delafossite pdcoo₂*, Phys. Rev. B **81**, 115120 (2010), doi:10.1103/PhysRevB.81.115120.
- [5] H.-J. Noh, J. Jeong, J. Jeong, E.-J. Cho, S. B. Kim, K. Kim, B. I. Min and H.-D. Kim, *Anisotropic electric conductivity of delafossite pdcoo₂ studied by*

- angle-resolved photoemission spectroscopy*, Phys. Rev. Lett. **102**, 256404 (2009), doi:10.1103/PhysRevLett.102.256404.
- [6] R. D. Shannon, D. B. Rogers, C. T. Prewitt and J. L. Gillson, *Chemistry of noble metal oxides. iii. electrical transport properties and crystal chemistry of abO_2 compounds with the delafossite structure*, Inorganic Chemistry **10**(4), 723 (1971).
- [7] A. P. Mackenzie, *The properties of ultrapure delafossite metals*, Reports on Progress in Physics **80**(3), 032501 (2017), doi:10.1088/1361-6633/aa50e5.
- [8] C. W. Hicks, A. S. Gibbs, A. P. Mackenzie, H. Takatsu, Y. Maeno and E. A. Yelland, *Quantum oscillations and high carrier mobility in the delafossite $pdCoO_2$* , Physical Review Letters **109**(11) (2012), doi:10.1103/physrevlett.109.116401.
- [9] V. Sunko, P. McGuinness, C. Chang, E. Zhakina, S. Khim, C. Dreyer, M. Konczykowski, H. Borrmann, P. Moll, M. König and et al., *Controlled introduction of defects to delafossite metals by electron irradiation*, Physical Review X **10**(2) (2020), doi:10.1103/physrevx.10.021018.
- [10] H. Usui, M. Ochi, S. Kitamura, T. Oka, D. Ogura, H. Rosner, M. W. Haverkort, V. Sunko, P. D. C. King, A. P. Mackenzie and K. Kuroki, *Hidden kagome-lattice picture and origin of high conductivity in delafossite $ptCoO_2$* , Phys. Rev. Materials **3**, 045002 (2019), doi:10.1103/PhysRevMaterials.3.045002.
- [11] M. D. Bachmann, A. L. Sharpe, A. W. Barnard, C. Putzke, M. König, S. Khim, D. Goldhaber-Gordon, A. P. Mackenzie and P. J. W. Moll, *Super-geometric electron focusing on the hexagonal fermi surface of $pdCoO_2$* , Nature Communications **10**(1) (2019), doi:10.1038/s41467-019-13020-9.
- [12] C. Putzke, M. D. Bachmann, P. McGuinness, E. Zhakina, V. Sunko, M. Konczykowski, T. Oka, R. Moessner, A. Stern, M. König, S. Khim, A. P. Mackenzie *et al.*, *h/e oscillations in interlayer transport of delafossites* (2019), 1902.07331.
- [13] H. Takatsu, S. Yonezawa, S. Fujimoto and Y. Maeno, *Unconventional anomalous hall effect in the metallic triangular-lattice magnet $pdCoO_2$* , Physical Review Letters **105**(13) (2010), doi:10.1103/physrevlett.105.137201.
- [14] H. Takatsu, J. J. Ishikawa, S. Yonezawa, H. Yoshino, T. Shishidou, T. Oguchi, K. Murata and Y. Maeno, *Extremely large magnetoresistance in the nonmagnetic metal $pdCoO_2$* , Phys. Rev. Lett. **111**, 056601 (2013), doi:10.1103/PhysRevLett.111.056601.
- [15] J. C. A. Prentice and A. I. Coldea, *Modeling the angle-dependent magnetoresistance oscillations of fermi surfaces with hexagonal symmetry*, Phys. Rev. B **93**, 245105 (2016), doi:10.1103/PhysRevB.93.245105.
- [16] J. M. Ziman, *Principles of the Theory of Solids*, Cambridge University Press, ISBN 9780521297332, doi:10.1017/CBO9781139644075 (1972).
- [17] F. Bloch, *Über die quantenmechanik der elektronen in kristallgittern*, Zeitschrift für physik **52**(7-8), 555 (1929).

- [18] S. Zhang, Q. Wu, Y. Liu and O. V. Yazyev, *Magnetoresistance from fermi surface topology*, Phys. Rev. B **99**, 035142 (2019), doi:10.1103/PhysRevB.99.035142.
- [19] K. Vilkelis and A. Akhmerov, *Bloch-Lorentz magnetoresistance oscillations in delafossites*, doi:10.5281/zenodo.4977422, This work was supported by the NWO VIDI Grant (016.Vidi.189.180), an ERC Starting Grant 638760 and European Union's Horizon 2020 research and innovation programme FE-TOpen Grant No. 828948 (AndQC). (2020).